RAA 2021 Vol. **21** No. **6**, 144(8pp) doi: 10.1088/1674-4527/21/6/144

http://www.raa-journal.org *http://iopscience.iop.org/raa*

***R**esearch in*
***A**stronomy and*
***A**strophysics*

Statistical investigation on the formation of sunspot light bridges

Fu-Yu Li[1], Yu-Hao Chen[2], Yong-Liang Song[3], Zhen-Yong Hou[1] and Hui Tian[1,3]

[1] School of Earth and Space Sciences, Peking University, Beijing 100871, China; *lifuyu@pku.edu.cn*
[2] Yunnan Observatories, Chinese Academy of Sciences, Kunming 650011, China
[3] Key Laboratory of Solar Activity, National Astronomical Observatories, Chinese Academy of Sciences, Beijing 100101, China; *ylsong@bao.ac.cn*

Received 2021 February 2; accepted 2021 March 25

Abstract Light bridges (LBs) are bright lanes that divide one sunspot umbra into two or more parts. Though frequently observed in sunspots, their formation mechanisms have rarely been studied and thus are not well understood. Here we present results from the first statistical investigation on the formation of LBs. Using observations with the Helioseismic and Magnetic Imager on board the Solar Dynamics Observatory, we identified 144 LBs within 71 active regions (ARs) over the whole year of 2014. The formation processes of these LBs can be categorized into three groups: penumbral intrusion (type-A), sunspot merging (type-B) and umbral-dot emergence (type-C). The numbers of events in these three categories are 74, 57 and 13, respectively. The duration of the LB formation process is mostly less than 40 hours, with an average of ∼20 hours. Most LBs have a maximum length of less than $20''$. For type-A LBs, we found a positive correlation between the LB length and the duration of the LB formation process, suggesting a similar speed of penumbral intrusion in different sunspots.

Key words: sunspots — Sun: photosphere — Sun: activity — Sun: evolution

1 INTRODUCTION

Light bridges (LBs) are among the most prominent substructures in sunspots. In photospheric observations of some sunspots, LBs usually appear as bright elongated structures across an umbra and divide the umbra into multiple parts. Observations have revealed different types of LBs. One type of LBs shows granule-like convective cells, called granular LBs (Lagg et al. 2014). There is another type of LBs named penumbral LBs, which resemble penumbral filaments and often show barb-like features aside (Louis et al. 2008; Rimmele 2008; Bharti 2015; Wang et al. 2018; Hou et al. 2020). Signatures of magnetoconvection, such as dark lanes and dark knots, have been frequently found in some narrow LBs based on recent high-resolution observations (Berger & Berdyugina 2003; Lites et al. 2004; Felipe et al. 2016; Zhang et al. 2018). The magnetic field on LBs is generally believed to be weaker and more inclined compared to the surrounding umbra (Leka 1997; Rimmele 1997, 2004; Falco et al. 2016). However, very strong magnetic field has been occasionally found on LBs. For instance, Castellanos Durán et al. (2020) detected the strongest magnetic field with a strength of 8.2 kG in an LB.

From chromospheric and transition region observations, several types of small-scale dynamic phenomena have been reported on LBs. One prominent phenomenon is the surge-like activity repeatedly occurring above LBs, called Hα surges, light wall oscillations, plasma ejections or chromospheric jets by various authors (Asai et al. 2001; Shimizu et al. 2009; Yang et al. 2015; Toriumi et al. 2015a; Su et al. 2016; Robustini et al. 2016; Reid et al. 2018; Humphries et al. 2020; Li et al. 2020; Kotani & Shibata 2020; Shen 2021). The surge-like activity appears to have at least two components: persistent up-and-down motions driven by the upward leakage of magnetoacoustic waves, and intermittent high-speed jets triggered by magnetic reconnection (Zhang et al. 2017; Hou et al. 2017; Tian et al. 2018). Lim et al. (2020) detected opposite magnetic polarities emerging and canceling on an LB. Such an observational signature might suggest the occurrence of magnetic reconnection between small-scale emerging flux and pre-existing field on the LB, which could result in intermittent jets (Louis et al. 2015; Yuan & Walsh 2016; Hou et al. 2017; Tian et al. 2018; Bai et al. 2019). In addition, photospheric vortices occurring at the edge of an LB were reported to be associated with subsequent ejections of chromospheric surges (Yang et al. 2019). Light

bridges are also known to host sub-arcsecond transient bright dots with transition region temperatures, which are likely related to coronal rain or small-scale energy release events around the loop footpoints (Tian et al. 2014; Kleint et al. 2014). More recently, Li et al. (2021) reported blob-like plasma ejections with a speed of $\sim$80 km s^{-1} from an oscillating bright front above an LB. Observations of these different types of dynamics on LBs have significantly advanced our understanding of magneto-convection under the condition of strong magnetic field (Schüssler & Vögler 2006) and magnetic reconnection in the partially ionized lower atmosphere of sunspots (Ni et al. 2020).

Though frequently observed in sunspots, the formation mechanisms of LBs have rarely been studied. Only a few case studies exisit in the literature. There are suggestions that LBs can form through field-free hot plasma intruding into the gappy umbral magnetic field or through large-scale magnetoconvection (Parker 1979; Rimmele 2004; Toriumi et al. 2015b). Katsukawa et al. (2007) suggested that the emergence of umbral dots (UDs) near the edges of penumbral filaments and the inward motion of these UDs to the umbral center are triggered by a buoyant penumbral flux tube as well as subphotospheric flows across the sunspot. They claimed that the intrusion of penumbral filaments can facilitate the emergence of a buoyant flux tube and ultimately form an LB. Louis et al. (2020) reported the formation of one LB associated with large-scale emerging flux, of which one end was outside the sunspot and the other one was gradually crossing the umbra. Besides penumbral intrusion, merging of sunspots can also lead to the formation of LBs. Zirin & Wang (1990) studied several LBs and found that a transient thin LB can form through merging of two spots with the same polarity or opposite polarities (forming δ-spots).

With only a few case studies, the formation mechanisms of LBs are not well understood. Here we present analysis results from the first statistical investigation on the formation of LBs. Our analysis reveals three types of LB formation processes.

2 OBSERVATIONS

Uninterrupted observations provided by the Helioseismic and Magnetic Imager (HMI, Schou et al. 2012) on board the Solar Dynamics Observatory (SDO, Pesnell et al. 2012) allow us to investigate in detail the formation and evolution of LBs. We thus took the HMI continuum images and magnetograms for our statistical analysis. We examined the data in the whole year of 2014, when the Sun was active. We used the JHelioviewer software (Müller et al. 2017) (also see the website at: `https://www.helioviewer.org`) and inspected HMI images with a cadence of 1 hour to select events of LB formation. The following criteria were used for event selection: (1) the forming LB should be well isolated from other LBs; (2) the whole LB formation process should be clearly visible on the front side of the solar surface. The second criterion has excluded many events that occur at locations close to the solar limb. Based on these criteria, we have selected 144 LBs in 71 ARs and characterized their formation processes.

For a subset of these selected events, we also plotted image sequences using the data in the 'hmi.Ic_720s' and 'hmi.M_720s' series. The time cadence and spatial resolution of the data are 720 s and 1″, respectively. Some images generated from these data are shown in Figures 1–3.

3 RESULTS AND DISCUSSION

By examining the HMI continuum images, we found that the formation processes of these LBs can be categorized into three groups: penumbral intrusion (type-A), sunspot merging (type-B) and umbral-dot emergence (type-C). The numbers of events in these three categories are 74, 57 and 13, respectively. Observational details such as the NOAA number of the resident AR, starting and ending times of the formation process, are shown in Table 1. For type-A events, the starting time was defined as the time when a bright structure starts to intrude from the penumbra to the umbra. For type-C events, the starting time refers to the time when the first UD associated with the subsequently formed LB appears. We did not write down the starting times for type-B events, since it is difficult to determine them. The ending time of the formation process refers to the time when both ends of an LB connect with the penumbra or the length of an LB stops increasing. Table 1 also lists the duration of the LB formation process, the length and width of each LB, and the sunspot group classification of the resident AR. The length and width of an LB were calculated at the ending time of its formation process. The length was defined as the distance between two ends of the LB. The width was calculated at its middle location.

3.1 LB Formation through Intrusion of Penumbra

Previous case studies have shown that LBs could form when some parts of the penumbrae intrude towards the umbrae (Katsukawa et al. 2007; Louis et al. 2020). It was unclear how common this process is. Our statistical investigation shows that about 51% of the identified events (74 events) fall into the category of type-A, suggesting that penumbral intrusion is the most common process responsible for the formation of LBs.

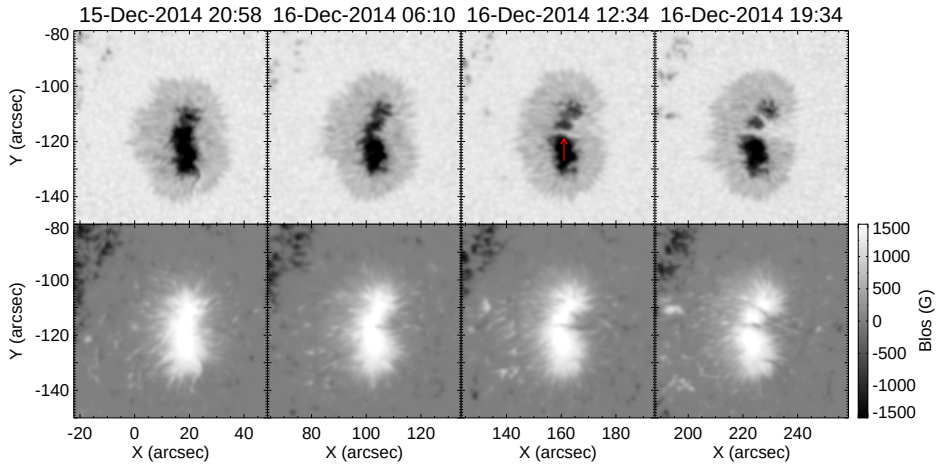

Fig. 1 The formation process of LB-64 (type-A). The top row shows HMI continuum images. The bottom row shows HMI line-of-sight (LOS) magnetograms. The *red arrow* indicates the location of the newly formed LB. An animation with the same field-of-view (FOV) is available at `http://www.raa-journal.org/docs/Supp/typeAmovie.mp4`, covering 40 hours starting at 17:58:09 UT on 2014 Dec 15.

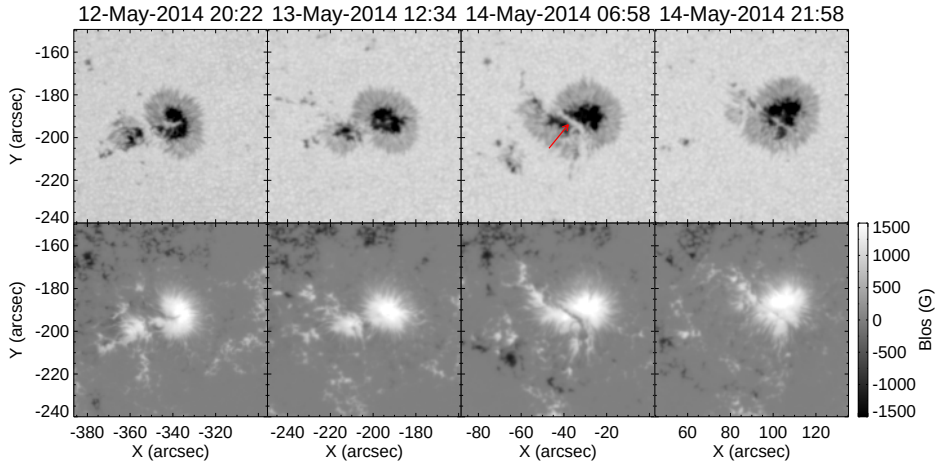

Fig. 2 The same as Fig. 1 but for LB-104 (type-B). An animation is available at `http://www.raa-journal.org/docs/Supp/typeBmovie.mp4`, covering 56 hours starting at 14:58:22 UT on 2014 May 12.

As an example, Figure 1 shows the formation process of LB-64 in the continuum intensity images and LOS magnetograms. At 20:58 UT on 2014 Dec 15, we can see that the umbra shows up as an elongated dark region. The longitudinal component of the magnetic field is the strongest in the umbra. At 06:10 UT on the next day, we can see a bright narrow structure intruding from the penumbra towards the umbra, around the location of X=105″ and Y=−118″. Around 12:00 UT, the intruding structure reaches the other side of the penumbra and a new LB forms. Almost simultaneously, another light bridge (LB-65) in the north part of the same sunspot is formed in the same way (see Fig. 1). A comparison between the continuum images and LOS magnetograms suggests that the LB is associated with an LOS magnetic field weaker than that of the surrounding umbra. At the time when the LB connects both sides of the inner boundary of the penumbra, we also observed a narrow lane of reduced LOS magnetic field strength at the location of the LB.

3.2 LB Formation through Sunspot Merging

Zirin & Wang (1990) found that some LBs can form when two or more sunspots/pores merge. Our statistical investigation shows that 57 LBs form through a similar process, which is about 40% of the total events. These events are categorized into type-B.

Figure 2 shows an example of type-B events. At 20:22 UT on 2014 May 12, we see two sunspots close to each other. There is an obvious gap between the two sunspots. Later, the distance between the two sunspots decreases. When the two spots collide, the gap and part of the

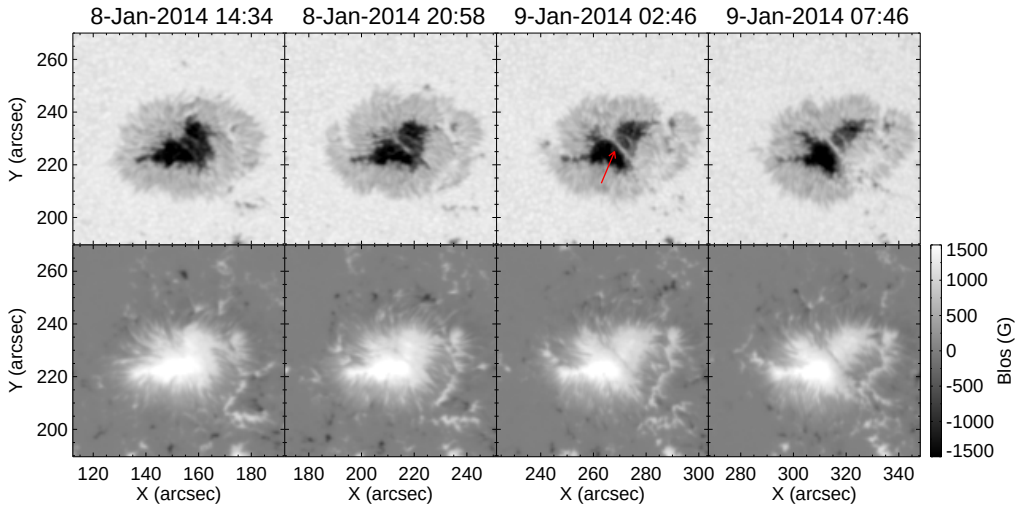

Fig. 3 The same as Fig. 1 but for LB-133 (type-C). An animation of this LB is also available at *http://www.raa-journal.org/docs/Supp/typeCmovie.mp4*, covering 34 hours starting at 09:58:09 UT on 2014 Jan 8.

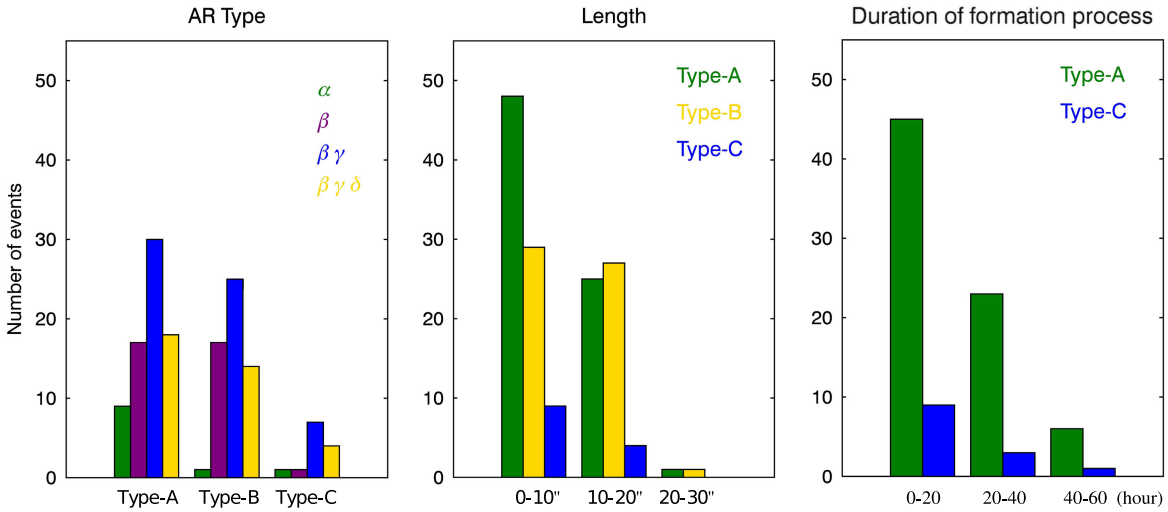

Fig. 4 Histograms of the sunspot group classification, LB length, and total duration of the LB formation process.

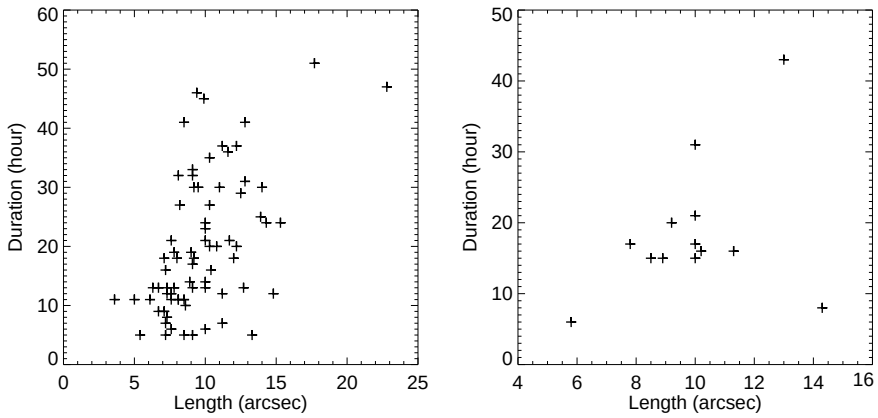

Fig. 5 Relationship between the LB length and formation duration for type-A (*left*) and type-C (*right*) events.

Table 1 Observational Details on the Formation Processes of the 144 Identified LBs

No.	Type	NOAA AR number	Starting Time (UT)	Ending Time (UT)	Duration (hour)	Length (arcsec)	Width (arcsec)	Hale Class
1	A	11944	2014/1/5 10:49	2014/1/7 14:09	51	17.7	1.0	$\beta\gamma\delta$
2	A	11944	2014/1/5 8:28	2014/1/7 7:09	47	22.8	2.0	$\beta\gamma\delta$
3	A	11944	2014/1/8 15:49	2014/1/9 5:49	14	8.9	1.4	$\beta\gamma\delta$
4	A	11946	2014/1/9 16:06	2014/1/10 5:28	13	12.7	2.8	$\beta\gamma$
5	A	11949	2014/1/15 14:32	2014/1/16 11:32	21	10.0	1.0	α
6	A	11960	2014/1/23 2:28	2014/1/24 11:22	33	9.1	1.0	α
7	A	11959	2014/1/19 4:42	2014/1/19 15:46	11	5.0	1.4	β
8	A	11967	2014/2/6 6:17	2014/2/6 16:32	10	8.6	1.4	$\beta\gamma\delta$
9	A	11974	2014/2/13 22:29	2014/2/14 11:29	13	6.7	1.0	$\beta\gamma\delta$
10	A	11977	2014/2/11 9:30	2014/2/12 3:29	18	12.0	2.0	β
11	A	11974	2014/2/15 22:09	2014/2/16 3:42	6	7.6	1.0	$\beta\gamma\delta$
12	A	11974	2014/2/16 3:42	2014/2/16 10:01	6	10.0	1.0	$\beta\gamma\delta$
13	A	11976	2014/2/17 14:14	2014/2/18 13:52	24	14.3	1.0	α
14	A	11981	2014/2/19 7:34	2014/2/19 15:10	8	7.3	1.0	β
15	A	11982	2014/2/26 23:16	2014/2/27 18:04	19	9.0	1.0	$\beta\gamma$
16	A	11987	2014/2/25 11:39	2014/2/25 16:36	5	7.2	1.4	$\beta\gamma$
17	A	11991	2014/3/1 10:13	2014/3/1 23:21	13	7.3	1.4	$\beta\gamma$
18	A	11991	2014/3/1 10:13	2014/3/1 23:21	13	10.0	2.2	$\beta\gamma$
19	A	11991	2014/3/6 11:31	2014/3/6 22:47	11	3.6	2.2	β
20	A	12002	2014/3/10 21:31	2014/3/11 2:59	5	8.5	1.4	$\beta\gamma\delta$
21	A	12010	2014/3/21 18:38	2014/3/23 0:49	32	8.1	1.0	$\beta\gamma$
22	A	12010	2014/3/23 20:53	2014/3/24 7:23	11	8.1	2.2	$\beta\gamma\delta$
23	A	12021	2014/3/30 22:54	2014/3/31 3:49	5	9.1	1.0	$\beta\gamma$
24	A	12026	2014/4/4 0:53	2014/4/4 8:17	7	7.2	2.2	$\beta\gamma$
25	A	12035	2014/4/13 7:57	2014/4/14 5:02	21	11.7	1.0	$\beta\gamma$
26	A	12034	2014/4/18 18:22	2014/4/19 3:33	9	6.7	1.0	β
27	A	12042	2014/4/19 23:27	2014/4/20 11:42	12	7.3	1.0	β
28	A	12036	2014/4/17 20:56	2014/4/18 6:07	9	7.1	1.0	$\beta\gamma$
29	A	12049	2014/5/2 10:22	2014/5/3 23:01	37	11.2	3.0	$\beta\gamma$
30	A	12049	2014/5/4 0:37	2014/5/4 18:42	18	7.1	1.0	β
31	A	12055	2014/5/8 12:58	2014/5/9 4:48	16	7.2	1.4	β
32	A	12055	2014/5/10 9:05	2014/5/11 14:41	30	11.0	1.4	$\beta\gamma$
33	A	12056	2014/5/10 0:18	2014/5/10 21:05	21	7.6	1.4	$\beta\gamma$
34	A	12056	2014/5/11 7:29	2014/5/11 18:41	11	8.5	2.0	$\beta\gamma$
35	A	12057	2014/5/11 1:09	2014/5/12 0:39	24	10.0	1.0	α
36	A	12060	2014/5/12 9:19	2014/5/12 20:27	11	8.1	2.0	$\beta\gamma$
37	A	12060	2014/5/16 15:09	2014/5/17 14:15	23	10.0	2.0	$\beta\gamma$
38	A	12061	2014/5/14 3:41	2014/5/16 1:47	46	9.4	1.0	α
39	A	12085	2014/6/10 0:14	2014/6/11 4:52	29	12.5	2.2	$\beta\gamma$
40	A	12104	2014/7/5 11:35	2014/7/6 15:05	27	10.3	2.2	$\beta\gamma$
41	A	12107	2014/7/2 4:32	2014/7/3 11:28	31	12.8	1.0	β
42	A	12127	2014/7/31 16:55	2014/8/1 4:05	11	7.6	1.0	$\beta\gamma$
43	A	12135	2014/8/7 2:23	2014/8/7 9:34	7	11.2	1.4	β
44	A	12146	2014/8/19 15:37	2014/8/20 7:27	16	10.4	1.0	α
45	A	12151	2014/8/24 23:52	2014/8/25 12:32	13	9.1	1.0	α
46	A	12151	2014/8/30 22:29	2014/9/1 15:29	41	8.5	1.4	β
47	A	12158	2014/9/6 17:25	2014/9/7 17:18	24	15.3	2.0	β
48	A	12157	2014/9/10 18:47	2014/9/12 6:06	35	10.3	1.4	$\beta\gamma\delta$
49	A	12157	2014/9/11 8:17	2014/9/12 11:28	27	8.2	1.4	$\beta\gamma\delta$
50	A	12157	2014/9/13 8:28	2014/9/14 14:39	30	9.5	1.0	$\beta\gamma$
51	A	12172	2014/9/26 4:27	2014/9/27 16:17	36	11.6	2.2	$\beta\gamma$
52	A	12172	2014/9/26 16:00	2014/9/27 11:40	20	10.8	1.4	$\beta\gamma$
53	A	12172	2014/9/26 16:00	2014/9/28 0:23	30	9.2	2.8	$\beta\gamma$
54	A	12186	2014/10/13 2:05	2014/10/14 10:32	32	9.1	1.0	β
55	A	12192	2014/10/25 14:48	2014/10/26 15:51	25	13.9	1.0	$\beta\gamma\delta$
56	A	12192	2014/10/27 15:45	2014/10/28 05:25	12	11.2	1.0	$\beta\gamma\delta$
57	A	12216	2014/11/22 00:05	2014/11/23 12:39	37	12.2	1.4	$\beta\gamma$
58	A	12216	2014/11/25 03:14	2014/11/26 23:55	45	9.9	1.4	$\beta\gamma$
59	A	12216	2014/11/28 02:19	2014/11/28 22:38	20	10.3	1.4	β
60	A	12222	2014/12/01 12:29	2014/12/02 00:58	12	14.8	1.0	$\beta\gamma$
61	A	12222	2014/12/04 01:03	2014/12/05 18:01	41	12.8	1.0	$\beta\gamma$
62	A	12227	2014/12/06 17:10	2014/12/07 10:59	18	8.0	2.0	α
63	A	12230	2014/12/12 09:25	2014/12/12 23:20	14	10.0	1.4	$\beta\gamma$
64	A	12235	2014/12/15 20:55	2014/12/16 12:34	17	9.1	2.0	β
65	A	12235	2014/12/16 08:10	2014/12/16 21:27	13	7.8	1.4	β
66	A	12236	2014/12/18 22:27	2014/12/19 11:43	13	6.3	2.0	α
67	A	12241	2014/12/16 07:10	2014/12/17 12:46	30	14.0	2.0	$\beta\gamma$

Table 1 *Continued.*

No.	Type	NOAA AR number	Starting Time (UT)	Ending Time (UT)	Duration (hour)	Length (arcsec)	Width (arcsec)	Hale Class
68	A	11944	2014/1/5 13:09	2014/1/6 7:49	19	7.8	1.4	$\beta\gamma\delta$
69	A	12002	2014/3/13 13:08	2014/3/13 18:12	5	13.3	1.0	$\beta\gamma\delta$
70	A	12002	2014/3/11 15:37	2014/3/12 9:08	18	9.2	3.0	$\beta\gamma\delta$
71	A	11974	2014/2/12 8:29	2014/2/12 19:34	11	6.1	1.0	$\beta\gamma\delta$
72	A	12034	2014/4/18 1:32	2014/4/18 13:46	12	7.6	1.4	β
73	A	12080	2014/6/9 20:17	2014/6/10 1:14	5	5.4	2.0	$\beta\gamma\delta$
74	A	12222	2014/12/02 06:18	2014/12/03 01:54	20	12.2	1.0	$\beta\gamma$
75	B	11936		2014/1/1 1:46		7.1	1.4	$\beta\gamma\delta$
76	B	11936		2014/1/1 0:00		7.3	1.0	$\beta\gamma\delta$
77	B	11944		2014/1/4 4:40		14.9	1.4	$\beta\gamma$
78	B	11944		2014/1/3 2:40		8.1	1.0	$\beta\gamma$
79	B	11944		2014/1/4 10:42		14.2	1.0	$\beta\gamma$
80	B	11968		2014/2/2 7:16		9.8	1.4	$\beta\gamma$
81	B	11967		2014/1/31 7:27		11.0	2.0	$\beta\gamma\delta$
82	B	11967		2014/2/7 10:28		27.1	2.0	$\beta\gamma\delta$
83	B	11973		2014/2/7 11:36		8.1	1.0	β
84	B	11974		2014/2/14 15:16		11.7	1.0	$\beta\gamma\delta$
85	B	11974		2014/2/15 16:37		14.3	1.4	$\beta\gamma\delta$
86	B	11982		2014/2/24 7:07		6.1	1.0	$\beta\gamma$
87	B	11982		2014/2/24 15:34		7.2	2.2	$\beta\gamma$
88	B	11984		2014/2/26 16:20		7.3	1.4	α
89	B	11991		2014/2/28 15:33		8.6	2.2	β
90	B	11996		2014/3/11 2:42		7.0	1.0	$\beta\gamma$
91	B	11996		2014/3/11 1:14		9.0	1.0	$\beta\gamma$
92	B	12003		2014/3/14 2:17		10.0	2.0	$\beta\gamma$
93	B	12004		2014/3/19 14:51		11.2	1.4	β
94	B	12011		2014/3/19 5:29		8.6	1.4	β
95	B	12011		2014/3/21 7:43		4.0	2.0	β
96	B	12014		2014/3/20 22:23		9.2	1.4	β
97	B	12021		2014/3/30 21:40		18.4	1.4	$\beta\gamma$
98	B	12021		2014/3/31 22:12		13.6	3.0	$\beta\gamma$
99	B	12038		2014/4/22 20:35		11.0	1.4	β
100	B	12036		2014/4/15 7:41		13.3	2.0	$\beta\gamma$
101	B	12047		2014/5/3 1:15		11.7	3.0	$\beta\gamma$
102	B	12049		2014/5/1 22:55		8.0	2.0	$\beta\gamma$
103	B	12055		2014/5/8 0:47		7.8	1.4	β
104	B	12060		2014/5/14 6:58		13.6	2.2	$\beta\gamma$
105	B	12080		2014/6/10 3:12		9.1	2.0	$\beta\gamma\delta$
106	B	12080		2014/6/10 13:04		16.1	1.4	$\beta\gamma\delta$
107	B	12085		2014/6/9 8:27		8.5	1.0	$\beta\gamma$
108	B	12085		2014/6/9 14:22		6.0	2.0	$\beta\gamma$
109	B	12108		2014/7/6 8:12		12.2	3.0	$\beta\gamma$
110	B	12119		2014/7/20 15:44		8.5	1.4	β
111	B	12126		2014/7/30 3:44		9.2	1.0	$\beta\gamma$
112	B	12132		2014/8/2 18:29		11.7	2.0	$\beta\gamma\delta$
113	B	12144		2014/8/16 19:04		11.0	1.0	$\beta\gamma$
114	B	12153		2014/9/2 21:14		9.0	1.0	β
115	B	12153		2014/9/4 5:53		11.0	2.0	β
116	B	12153		2014/9/4 16:47		10.8	1.4	β
117	B	12152		2014/9/3 16:02		10.6	1.4	$\beta\gamma$
118	B	12175		2014/9/27 8:11		12.1	1.4	$\beta\gamma\delta$
119	B	12175		2014/9/27 20:55		13.4	2.2	$\beta\gamma\delta$
120	B	12172		2014/9/28 6:10		12.4	2.0	$\beta\gamma$
121	B	12193		2014/10/20 13:38		10.3	2.2	β
122	B	12193		2014/10/22 6:57		7.8	1.4	β
123	B	12203		2014/11/02 10:46		10.8	2.0	β
124	B	12230		2014/12/11 00:22		9.1	2.0	$\beta\gamma$
125	B	12234		2014/12/12 16:23		9.5	2.0	$\beta\gamma$
126	B	12242		2014/12/17 08:40		18.0	2.2	$\beta\gamma\delta$
127	B	12242		2014/12/17 10:43		15.6	2.2	$\beta\gamma\delta$
128	B	11959		2014/1/19 21:52		9.5	2.0	β
129	B	12002		2014/3/11 9:05		6.1	2.0	$\beta\gamma\delta$
130	B	12038		2014/4/22 6:32		5.8	1.4	β
131	B	12241		2014/12/16 20:25		17.0	1.4	$\beta\gamma$
132	C	11944	2014/1/10 2:49	2014/1/10 23:49	21	10.0	1.0	$\beta\gamma\delta$
133	C	11946	2014/1/8 10:34	2014/1/9 2:49	16	11.3	1.4	$\beta\gamma$
134	C	11946	2014/1/9 6:58	2014/1/10 0:00	17	7.8	1.4	$\beta\gamma$

Table 1 *Continued.*

No.	Type	NOAA AR number	Starting Time (UT)	Ending Time (UT)	Duration (hour)	Length (arcsec)	Width (arcsec)	Hale Class
135	C	11974	2014/2/11 22:29	2014/2/12 4:29	6	5.8	2.0	$\beta\gamma\delta$
136	C	12033	2014/4/14 10:22	2014/4/15 17:46	31	10.0	1.4	α
137	C	12056	2014/5/11 5:59	2014/5/11 21:02	15	8.5	1.0	$\beta\gamma$
138	C	12056	2014/5/11 3:49	2014/5/11 11:19	8	14.3	1.0	$\beta\gamma$
139	C	12157	2014/9/7 13:02	2014/9/8 5:32	17	10.0	2.0	$\beta\gamma\delta$
140	C	12172	2014/9/26 16:41	2014/9/27 8:41	16	10.2	2.0	$\beta\gamma$
141	C	12193	2014/10/22 17:37	2014/10/23 8:17	15	8.9	1.0	$\beta\gamma$
142	C	12209	2014/11/19 17:05	2014/11/21 12:34	43	13.0	1.0	$\beta\gamma\delta$
143	C	11960	2014/1/24 16:44	2014/1/25 7:16	15	10.0	1.4	β
144	C	12222	2014/12/01 12:18	2014/12/02 08:05	20	9.2	1.0	$\beta\gamma$

penumbrae close to the gap are squeezed. As the two spots completely merge into one spot, the region between the two approaching umbrae evolves into an LB. The LOS magnetic field associated with the LB is also evidently weaker than that of the umbral regions on both sides.

For type-B events, it is difficult to identify the starting time of the formation process. So the starting time and the durations of the type-B events are not listed in Table 1.

3.3 LB Formation through Umbral-dot Emergence

Previous observations have revealed the presence of UDs near the leading edges of intruding penumbral structures (Katsukawa et al. 2007; Rimmele 2004; Ortiz et al. 2010). However, it was unclear whether the emergence of UDs in the center of a sunspot can facilitate the formation of an LB. We identified 13 events where the formation of LBs appears to be preceded by the emergence of aligned UDs within the umbrae. These events are categorized into type-C. About 9% of our samples fall into this category.

As an example, Figure 3 shows four snapshots taken at different stages of the formation process of the LB-133. Starting from about 10:34 UT on 2014 Jan 8 (see the associated online animation), we see the emergence of several isolated UDs in the center of the umbra of a sunspot. After the first appearance, these UDs start to connect with each other and evolve into extensive bright features. Simultaneously, the penumbras also have a trend to intrude into the umbra. Roughly 16 hours later, the extensive structures evolved from the UDs and the intruding penumbral structure connect, forming an LB. In the meantime, the LOS magnetic field strength shows a decrease at the location of the LB. Though penumbral intrusion was also identified in this case, we did not classify this event into type-A because the behavior described above appears to be different from that of type-A events, in which an intruding structure continuously moves towards the other side of a sunspot and forms the whole or main body of an LB. We would like to mention that the penumbral intrusion is not always identified. About half of the type-C events only reveal the emergence and alignment of UDs during the LB formation process, and there is no obvious signature of penumbral intrusion in these events.

It is believed that UDs and LBs have a similar cusp-like magnetic field structure above the visible solar surface (Rimmele 2008, 1997; Schüssler & Vögler 2006; Ortiz et al. 2010; Cheung et al. 2010). Considering the similar magnetic field topology, it is not difficult to understand that the emergence and alignment of UDs could lead to the formation of LBs. It is also possible that the appearance of UDs well inside an umbra weakens the umbral magnetic field and thus facilitates the emergence of a buoyant flux tube (Louis et al. 2020; Katsukawa et al. 2007; Rimmele 1997).

3.4 Statistic Analysis

Figure 4 presents the distributions of the sunspot group classification, LB length, and total duration of the LB formation process (see the details in Table 1). From the left panel of Figure 4, we can see that most LBs are formed in complicated ARs that are associated with $\beta\gamma$ or $\beta\gamma\delta$ sunspot groups. Only 11 events are identified in unipolar ARs with α sunspot group. Out of these 11 events, nine belong to type-A.

The average lengths of the LBs are $9.8''\pm3.0''$, $10.7''\pm3.8''$ and $9.9''\pm2.2''$ for type-A, type-B and type-C events, respectively. After dividing the lengths into three intervals ($0''$–$10''$, $10''$–$20''$ and $20''$–$30''$), we present in the middle panel of Figure 4 the distributions of the lengths for different types. We found that for each type more than half LBs are shorter than $10''$, and only a few LBs are longer than $20''$.

The distributions of the LB formation duration for type-A and type-C events are presented in the right panel of Figure 4. The average formation durations for the type-A and type-C events are 20 ± 12 and 18 ± 10 hours, respectively. Most LBs form within 40 hours, and the number of events obviously decreases with the increased formation duration.

We also investigated the relationships between different parameters for type-A and type-C events. Two scatter

plots are shown in Figure 5. There appears to be a positive correlation between the LB length and formation duration. For type-A events their correlation coefficient is about 0.53, which is significant at the 99.9% confidence level (Bevington & Robinson 2003). This correlation suggests that the speed of penumbral intrusion is nearly the same in different sunspots. For the type-C events, this correlation is not as significant as that for the type-A events.

4 SUMMARY

Based on SDO/HMI observations in the year of 2014, we have performed a statistical investigation on the formation of sunspot LBs for the first time. We have categorized the formation processes of 144 LBs into three groups: penumbral intrusion (type-A), sunspot merging (type-B) and umbral-dot emergence (type-C). The percentages of these three groups are 51%, 40% and 9%, respectively.

Most of the identified LBs are formed in ARs with $\beta\gamma$ and $\beta\gamma\delta$ sunspot groups. The duration of the LB formation process is less than 40 hours for most LBs, and the average is about 20 hours. The maximum lengths of most identified LBs are less than $20''$. For type-A events, we found a positive correlation between the formation period and length, suggesting that the speed of penumbral intrusion is almost the same for different LBs. The correlation is less obvious for type-C events.

Acknowledgements This work was supported by the National Natural Science Foundation of China (Grant Nos. 11803002, 11825301 and 11790304) and the Strategic Priority Research Program of Chinese Academy of Sciences (XDA17040507). HMI is an instrument onboard the Solar Dynamics Observatory, a mission for NASA's Living With a Star program.

References

Asai, A., Ishii, T. T., & Kurokawa, H. 2001, ApJL, 555, L65
Bai, X., Socas-Navarro, H., Nóbrega-Siverio, D., et al. 2019, ApJ, 870, 90
Berger, T. E., & Berdyugina, S. V. 2003, ApJL, 589, L117
Bevington, P. R., & Robinson, D. K. 2003, Data Reduction and Error Analysis for the Physical Sciences, eds, Philip, R. B., & Keith, D. R. (Boston, MA: McGraw-Hill)
Bharti, L. 2015, MNRAS, 452, L16
Castellanos Durán, J. S., Lagg, A., Solanki, S. K., et al. 2020, ApJ, 895, 129
Cheung, M. C. M., Rempel, M., Title, A. M., et al. 2010, ApJ, 720, 233
Falco, M., Borrero, J. M., Guglielmino, S. L., et al. 2016, Sol. Phys., 291, 1939
Felipe, T., Collados, M., Khomenko, E., et al. 2016, A&A, 596, A59
Hou, Y., Zhang, J., Li, T., et al. 2017, ApJL, 848, L9
Hou, Y. J., Li, T., Zhong, S. H., et al. 2020, A&A, 642, A44
Humphries, L. D., Verwichte, E., Kuridze, D., et al. 2020, ApJ, 898, 17
Katsukawa, Y., Yokoyama, T., Berger, T. E., et al. 2007, PASJ, 59, S577
Kleint, L., Antolin, P., Tian, H., et al. 2014, ApJL, 789, L42
Kotani, Y., & Shibata, K. 2020, PASJ, 72, 75
Lagg, A., Solanki, S. K., van Noort, M., et al. 2014, A&A, 568, A60
Leka, K. D. 1997, ApJ, 484, 900
Lim, E.-K., Yang, H., Yurchyshyn, V., et al. 2020, ApJ, 904, 84
Lites, B. W., Scharmer, G. B., Berger, T. E., et al. 2004, Sol. Phys., 221, 65
Li, T., Hou, Y., Zhang, J., et al. 2020, MNRAS, 492, 2510
Li, F., Chen, Y., Hou, Y., et al. 2021, ApJ, 908, 201
Louis, R. E., Bayanna, A. R., Mathew, S. K., et al. 2008, Sol. Phys., 252, 43
Louis, R. E., Bellot Rubio, L. R., de la Cruz Rodríguez, J., et al. 2015, A&A, 584, A1
Louis, R. E., Beck, C., & Choudhary, D. P. 2020, ApJ, 905, 153
Müller, D., Nicula, B., Felix, S., et al. 2017, A&A, 606, A10
Ni, L., Ji, H., Murphy, N. A., et al. 2020, Proceedings of the Royal Society of London Series A, 476, 20190867
Ortiz, A., Bellot Rubio, L. R., & Rouppe van der Voort, L. 2010, ApJ, 713, 1282
Parker, E. N. 1979, ApJ, 234, 333
Pesnell, W. D., Thompson, B. J., & Chamberlin, P. C. 2012, Sol. Phys., 275, 3
Reid, A., Henriques, V. M. J., Mathioudakis, M., et al. 2018, ApJL, 855, L19
Rimmele, T. R. 1997, ApJ, 490, 458
Rimmele, T. R. 2004, ApJ, 604, 906
Rimmele, T. 2008, ApJ, 672, 684
Robustini, C., Leenaarts, J., de la Cruz Rodriguez, J., et al. 2016, A&A, 590, A57
Schou, J., Scherrer, P. H., Bush, R. I., et al. 2012, Sol. Phys., 275, 229
Schüssler, M. & Vögler, A. 2006, ApJL, 641, L73
Shen, Y. 2021, Proceedings of the Royal Society of London Series A, 477, 217
Shimizu, T., Katsukawa, Y., Kubo, M., et al. 2009, ApJL, 696, L66
Su, J. T., Ji, K. F., Banerjee, D., et al. 2016, ApJ, 816, 30
Tian, H., Kleint, L., Peter, H., et al. 2014, ApJL, 790, L29
Tian, H., Yurchyshyn, V., Peter, H., et al. 2018, ApJ, 854, 92
Toriumi, S., Katsukawa, Y., & Cheung, M. C. M. 2015a, ApJ, 811, 137
Toriumi, S., Cheung, M. C. M., & Katsukawa, Y. 2015b, ApJ, 811, 138
Wang, H., Liu, R., Li, Q., et al. 2018, ApJL, 852, L18
Yang, H., Lim, E.-K., Iijima, H., et al. 2019, ApJ, 882, 175
Yang, S., Zhang, J., Jiang, F., et al. 2015, ApJL, 804, L27
Yuan, D., & Walsh, R. W. 2016, A&A, 594, A101
Zhang, J., Tian, H., He, J., et al. 2017, ApJ, 838, 2
Zhang, J., Tian, H., Solanki, S. K., et al. 2018, ApJ, 865, 29
Zirin, H., & Wang, H. 1990, Sol. Phys., 125, 45